RESEARCH ARTICLE | AUGUST 13 2024

Photoluminescence study of MgGa₂O₄ spinel oxide films grown by molecular beam epitaxy ⊘

Tianchen Yang ^[]; Chengyun Shou ^[]; Jason Tran; Abdullah Almujtabi ^[]; Quazi Sanjid Mahmud ^[]; Edward Zhu; Yuan Li ^[]; Peng Wei ^[]; Jianlin Liu ^[]



Appl. Phys. Lett. 125, 071903 (2024) https://doi.org/10.1063/5.0218242

A CHORUS





Articles You May Be Interested In

Insights of phosphor charging upon exposure to intense illumination

Appl. Phys. Lett. (December 2024)





Photoluminescence study of MgGa₂O₄ spinel oxide films grown by molecular beam epitaxy

Cite as: Appl. Phys. Lett. **125**, 071903 (2024); doi: 10.1063/5.0218242 Submitted: 9 May 2024 · Accepted: 31 July 2024 · Published Online: 13 August 2024







AFFILIATIONS

Department of Electrical and Computer Engineering, University of California, Riverside, California 92521, USA

ABSTRACT

As a promising ultrawide bandgap oxide semiconductor material in the spinel family, magnesium gallate $(MgGa_2O_4)$ exhibits great potential applications in power electronics, transparent electronics, and deep ultraviolet optoelectronics. However, few studies reveal its photoluminescence (PL) properties. In this work, $MgGa_2O_4$ films were grown by using oxygen plasma assisted molecular beam epitaxy. The bandgap of $MgGa_2O_4$ spinel films is determined to be around $5.4-5.5\,\text{eV}$, and all samples have transmittance over 90% in the visible spectral range. X-ray diffraction patterns confirmed that the spinel films were grown highly along $\langle 111 \rangle$ oriented. Power and temperature dependent PL studies were investigated. Optical transitions involving self-trapped hole, oxygen vacancy deep donor, and magnesium atom on gallium site deep acceptor levels were revealed.

Published under an exclusive license by AIP Publishing. https://doi.org/10.1063/5.0218242

With the properties of transparency to visible light, transparent semiconducting oxides (TSOs) of optical bandgap larger than \sim 3 eV have great potential in electronic and optoelectronic applications, such as deep ultraviolet (UV) photodetectors, photodiodes, Schottky diodes, and transparent thin film transistors. ^{1,2} Among these TSO materials, ZnO, ^{3,4} In_2O_3 , ⁵ SnO_2 , ^{6,7} and Ga_2O_3 , are extensively studied. Previously, we explored the possibility of Ga₂O₃ with Mg incorporation in the beta phase for deep UV photodetector applications. 10,11 MgGaO ultrawide bandgap engineering with normalized Mg at. %/Ga at.% ranging from 0%/100% to 100%/0% was investigated for the study of phase transition and optical properties as well.¹² Among all different element composition combinations, it is reported that the inverse spinel magnesium gallate (MgGa2O4) of normalized Mg at. %/Ga at. % at 33.33%/66.67% is applicable for solar blind photodetector applications^{13–15} due to its reported large bandgap (4.7–5.36 eV) at room temperature, 14,15 good mechanical properties, high radiation hardness,14 and high thermal chemical stability at high temperature. 16,17 Meanwhile, as a good luminescent material, the MgGa₂O₄ luminescence properties were studied with the incorporation of Mn²⁺ for green, 18,19 Eu³⁺ for red, 19,20 and Cr³⁺ and Ni⁺ for near-infrared light emission. 21-24 Nevertheless, there are only very few room temperature photoluminescence (PL) studies of native defects in MgGa₂O₄ itself to illustrate the PL mechanism, ^{25,26} in contrast to extensive PL

studies of β -Ga₂O₃ with/without Mg doped. ^{27–29} In addition, MgGa₂O₄ is mostly produced by the Czochralski method^{2,30} or high-temperature solid reaction methods^{31–33} as bulk materials. Toward electronic and optoelectronic device applications, a few epitaxial film growth attempts are reported recently by metalorganic chemical vapor deposition (MOCVD)^{13,15} or pulsed laser deposition (PLD)¹⁴ methods. As an alternative precise growth control method, molecular beam epitaxy (MBE) has not been used for MgGa₂O₄ growth yet. In this study, MgGa₂O₄ epitaxial films were grown by MBE. The structural, optical, and surface morphology properties were studied. In particular, comprehensive PL studies including power dependent and temperature dependent PL were carried out. The PL mechanism involving optical transitions through self-trapped hole (STH), oxygen vacancy deep donor, and Mg on Ga site deep acceptor energy levels is revealed in spinel MgGa₂O₄, compared to a reference β -Ga₂O₃ sample.

 $MgGa_2O_4$ films were grown on two-inch c-sapphire substrates by using an RF oxygen plasma assisted MBE system (SVT Associates, Inc.). Piranha solution (H_2O_2 : $H_2SO_4=3.5$) at 200 °C was used to clean substrate for about 20 min, followed by de-ionized water rinse process. After dried by nitrogen gas, substrate was transferred to the loadlock chamber of MBE immediately. Mg (4N) and Ga shots (6N) (Alfa Aesar) high-purity elemental sources in effusion cells were used for sample growth. To achieve an atomic level surface at a high vacuum

 $^{^{2}}$ Department of Physics and Astronomy, University of California, Riverside, California 92521, USA

a) Author to whom correspondence should be addressed: jianlin@ece.ucr.edu. Tel.: 1-9518277131. Fax: 1-9518272425

of 10⁻⁹ Torr, a pre-growth substrate annealing process was performed at 800 °C for 20 min. The Ga and Mg effusion cell temperature was fixed at 750 and 410 °C, respectively. The growth temperature for spinel samples #2-#4 was set as 400, 500, and 600 °C, respectively, while it was set at 600 °C for reference beta phase Ga₂O₃ sample #1. Meanwhile, 2.0 sccm flux of oxygen under 400 W RF plasma was introduced for 5 h. Then, a post-growth annealing process without oxygen atmosphere was operated at 700 °C for 20 min. The growth conditions are listed in Table S1 of the supplementary material. The film thickness was measured by a Veeco Dektak 8 profilometer, yielding \sim 364.35, \sim 981.18, \sim 1122.36, and \sim 1217.86 nm for samples #1-#4, respectively, as shown in Table S1 of the supplementary material. Mg, Ga, and O compositions of all samples were measured by energy-dispersive x-ray (EDX) in a TESCAN SBH scanning electron microscope (SEM). For film phase determination, film quality, epitaxial relationship, and lattice constant investigation, x-ray diffraction (XRD) theta-2theta, rocking curve, in-plane phi scan, and reciprocal space mapping (RSM) of the samples were measured by using a Bruker D8 Advance x-ray diffractometer and a Rigaku SmartLab x-ray diffractometer with Cu K α ($\lambda = 0.15405$ nm) radiation at room temperature, respectively. Absorption and transmittance spectra were measured using a high-performance UV-Vis-NIR spectrophotometer (Cary 5000, Agilent Inc.). PL spectra were measured with a home-built PL system, which is equipped with a 193-nm ArF excimer laser.

Figure 1(a) shows EDX spectra of the four samples. Similar to the reported MgGa₂O₄ EDX spectra, ¹³ the O k α , Ga L α , and Mg K α peaks are located around 0.525, 1.098, and 1.253 keV, respectively, and Al signal from the substrate is undetected due to the large film thickness.

As listed in Table S1 in the supplementary material, Ga at.%/O at. % of sample #1 is 40.05%/59.95%, while Mg at. %/Ga at.%/O at. % is 15.26%/27.71%/57.03%, 14.62%/27.60%/57.78%, and 14.25%/28.58%/57.17% for samples #2, #3, and #4, respectively. Element atomic ratios of all three spinel samples are close to the nominal value of spinel MgGa₂O₄,³⁴ namely, 14.28%/28.57%/57.15%, although Mg at. % decreases slightly with the increase in the substrate temperature. The cross-sectional SEM image of sample #4 is shown in Fig. 1(b), while the images of other samples are shown in Figs. S1(a)–S1(c) of the supplementary material. The results indicate that the films grow epitaxially well with substrate, and the film thickness of the samples matches the values measured by a profilometer. SEM surface morphology of sample #4 in Fig. 1(c) and samples #1–#3 in Figs. S1(d)–S1(f) indicate the smooth surface for all samples.

Figure 1(d) shows the XRD pattern in the $\theta/2\theta$ scan mode of all four samples. Compared to the clear monoclinic structure of sample #1 with three typical diffraction peaks ($\bar{2}01$), ($\bar{4}02$), and ($\bar{6}03$), $^{10-12}$ which are located at \sim 19.12°, 38.50°, and 59.14°, respectively, three diffraction peaks located at \sim 35.93°, 37.59°, and 80.24° correspond to the spinel phases of (311), (222), and (444) in samples #2–#4, respectively. $^{15,33-35}$ According to Bragg's law, the d-spacing value of (222) plane is calculated to be \sim 2.390 Å; therefore, the lattice constant $a_{\rm spinel}$ is $2\sqrt{3}d_{(222)}$, namely, 8.282 Å, which is in good agreement with the nominal value of 8.288 Å reported in MgGa₂O₄ PDF 00-010-0133. The inset of Fig. 1(d) is a schematic of spinel MgGa₂O₄ structure with two kinds of Ga atoms located in both tetrahedral and octahedral sites, while the Mg atom locates only in octahedral site, namely, $Ga^{\rm tet}(MgGa)^{\rm oct}O_4$. The (111) plane is marked to indicate more

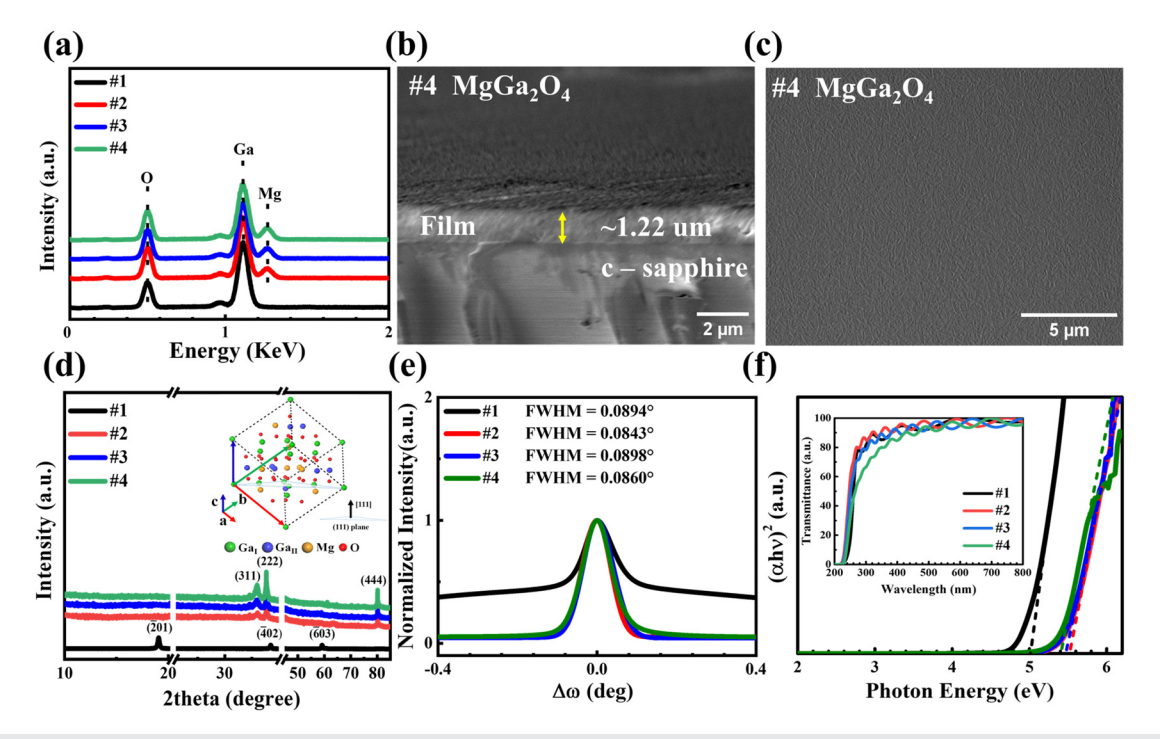


FIG. 1. (a) EDX spectra of β -Ga₂O₃ and spinel MgGa₂O₄ thin films. (b) SEM cross section and (c) surface morphology image of sample #4. (d) XRD pattern in the theta-2theta scan mode (inset is the spinel structure schematic). (e) Normalized XRD rocking curves for β -Ga₂O₃ ($\bar{4}$ 02) and spinel MgGa₂O₄ (222) peaks. (f) Tauc plot of absorption spectra (inset is the transmittance spectra).

preferred $\langle 111 \rangle$ growth orientation with respect to $\langle 311 \rangle$ direction in the spinel sample. Figure 1(e) shows normalized XRD rocking curves for $\beta\text{-}\text{Ga}_2\text{O}_3$ (402) and spinel MgGa $_2\text{O}_4$ (222) peaks. The full width at half maximum (FWHM) of the curves for samples #1–#4 is recorded as 0.0894°, 0.0843°, 0.0898°, and 0.0860°, respectively. The small values indicate that the films have very good quality. Spinel MgGa $_2\text{O}_4$ film thickness dependent experiment was also carried out, as shown in Table S2 and Fig. S2 in the supplementary material, revealing single crystallinity.

Figure 1(f) shows absorption spectra of the samples. Both β -Ga₂O₃ and spinel MgGa₂O₄ are reported to be direct bandgap semiconductors. ^{10,12–15} Thus, the Tauc equation is expressed as $(\alpha hv)^2 = A(hv - E_g)$, where α is the absorption coefficient, h v is the energy, A is a proportionality constant. By extrapolating the linear segment of absorption spectra to intersect the hv-axis with a fitting straight line, the bandgap was extracted as 5.02 eV for sample #1 β -Ga₂O₃, and 5.52, 5.47, and 5.41 eV for spinel samples #2, #3, and #4, respectively, which is similar to the reported undoped MgGa₂O₄ bandgap 5.36 eV. ²³ The bandgap decreases with the increase in the substrate temperature due to less Mg incorporation. ³⁵ The inset transmittance spectra in Fig. 1(f) indicate that ~90% transmittance of light at the visible region was observed across the spectra for all samples.

Figure 2(a) shows the room temperature PL spectra at an incident power density of 12.8 mW/cm² for β -Ga₂O₃ sample #1 and spinel MgGa₂O₄ samples #2–#4. All spectra show broad luminescence³⁷ with main peak at maximum intensity located at \sim 409.99 nm for β -Ga₂O₃, \sim 428.01, 431.01, and 453.99 nm for spinel samples, respectively. Room temperature PL peak deconvolution was performed to extract the optical transitions of all samples. PL deconvoluted peaks of spinel MgGa₂O₄ sample #4 are shown in Fig. 2(b), which are \sim 3.28 eV for UV_I emission, $\sim 4.18\,eV$ for UV_{II} emission, $\sim 3.09\,eV$ for violet, \sim 2.67 eV for blue, and \sim 2.30 eV for green emissions, respectively. The PL peak deconvolutions for the other two spinel samples (samples #2 and #3) and the reference β -Ga₂O₃ sample #1 are shown in Figs. S3 and S4 in the supplementary material, respectively. An energy level diagram of the PL mechanism of spinel MgGa₂O₄ films is illustrated in Fig. 2(c). Self-trapped holes into polaron states are widely existed in wide bandgap oxides; 38-40 thus, UV_I emission of spinel MgGa₂O₄ is due to the recombination of electrons in the conduction band and STHs. Assuming the polaronic STH energy level E_{polaron}^{STH} is the same as that of β -Ga₂O₃, namely, it is located at \sim 1.1 eV above the valence

band, the UV_I emission can be calculated as $E_{UV_I} = E_g$ $-E_{\text{polaron}}^{STH} - E_{\text{STH}}^{\text{bind}}$, where E_g is the bandgap and $E_{\text{STH}}^{\text{bind}}$ is the selftrapping energy or the binding energy of STH to oxygen atom. Ebind E_{STH}^{bind} is estimated to be \sim 1.20, 1.10, and 1.03 eV for samples #2-#4, respectively. Compared to the reported self-trapped hole delocalization energy of $0.53\,\mathrm{eV}$ for $\beta\text{-Ga}_2\mathrm{O}_3$, ^{41,42} this deviation indicates that the localization of STHs is stronger in spinel MgGa2O4 than that of β -phase Ga₂O₃. Nevertheless, it could also be due to the different STH positions in spinel MgGa₂O₄ compared to β-Ga₂O₃, which requires further investigation. Considering the relative at. % of Mg to Ga in spinel samples, UVIII emission may be ascribed to the radiative recombination of electrons in the conduction band and holes occupied in antisite Mg_{Ga} deep acceptor levels. ^{39,40} Mg_{Ga} acceptor level in our spinel sample can be calculated as $E_{Mg_{Ga}}=E_{g}-E_{UV_{II}}$, where E_{g} is the bandgap at room temperature of $5.41\,\mathrm{eV}$, the $\mathrm{UV_{II}}$ emission energy $E_{UV_{II}}$ is 4.18 eV, so the $E_{Mg_{Ga}}$ was estimated as \sim 1.23 eV above the valence band for sample #4. The $E_{Mg_{Ga}}$ values for the other two MgGa₂O₄ samples 2 and 3 are also estimated as \sim 1.23 and 1.24 eV, respectively. These values are essentially fallen into theoretically calculated range of 1.0-1.5 eV.²⁹ In addition, three oxygen vacancy related donor defects levels in MgGa₂O₄ have been reported as that are in β-Ga₂O₃;^{25,43} therefore, violet, blue, and green emissions of spinel samples may be ascribed to the transition from the three oxygen vacancy donor bands to MgGa antisite deep acceptor levels, respectively. Using similar donor-acceptor-pair (DAP) energy calculation in ZnO,44 it leads to an estimation of three oxygen vacancy levels of 1.09, 1.51, and 1.88 eV below the conduction band minimum (CBM) for sample #4, respectively. For samples #2 and #3, the respective oxygen vacancy levels below the CBM are 1.48, 1.76, and 2.01 eV, and 1.33, 1.55, and 1.80 eV, respectively. These values are comparable with the reported oxygen vacancy levels in β -Ga₂O₃, namely, 1.38, 1.56, and 1.76 eV below the CBM. 43 It should be noted that violet, blue, and green emissions were previously designated from the optical transitions from oxygen vacancy donor bands to Ga or Mg vacancies acceptor levels in MgGa₂O₄ samples.^{26,45} Nevertheless, by incorporating more Mg atoms into spinel MgGa₂O₄ through substrate temperature control, these excess Mg atoms with respect to the nominal value would go to Ga sites, namely, MgGa antisites shall be the dominant acceptor states in our MgGa₂O₄ spinel samples, and these deep acceptors instead of Ga or Mg vacancies are assumed to have participated the observed visible transitions.

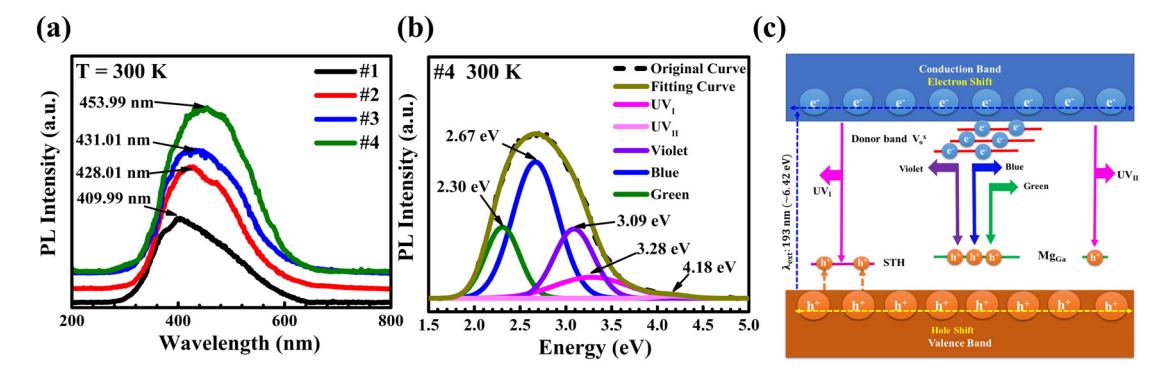


FIG. 2. (a) Room temperature PL spectra of β-Ga₂O₃ and spinel MgGa₂O₄ samples. (b) PL peak deconvolution of sample #4. (c) Schematic energy level diagram illustrating optical transitions in spinel MgGa₂O₄.

The deconvoluted PL peaks of β -Ga₂O₃ reference sample, as shown in Fig. S4(a) in the supplementary material, are \sim 3.43 eV for UV₁ emission, \sim 3.07 eV for violet, \sim 2.59 eV for blue, and \sim 2.35 eV for green emissions, respectively. An energy level diagram of the PL mechanism of β -Ga₂O₃ is illustrated as Fig. S4(b). The UV₁ peak is ascribed to be the recombination between electrons in the conduction band and holes bound to the STH energy level, which is similar to the reported STH PL peak of Ga₂O₃ at 3.4 eV. Thus, E_{STH}^{bind} was calculated as \sim 0.49 eV, which is close to the reported self-trapped hole delocalization energy of 0.53 eV for β -Ga₂O₃. The violet, blue, and green emissions are DAP transitions between oxygen vacancy donor bands and Ga vacancy/O vacancy defect complex (V_{Ga-O}) acceptor bands in Ga₂O₃. Another UV peak (UV_{II}), which is related to the V_{Ga-O} defect complex and is observed at power-dependent and temperature-dependent PL in the Ga₂O₃ sample as shown later, is complementary with this designation.

Figures 3(a)-3(d) show the power dependent PL spectra of samples #1-#4 at 14 K with an excitation power density from 12.8 to 51.2 mW/cm². The PL peak position for all samples does not show obvious change as the incident power density changes. Figures 3(e)-3(h) show integrated PL intensity of samples #1-#4 at 14K against incident power density. The integrated PL intensity increases with the incident power density due to the increased number of pumped electrons, which exhibits a similar nonlinear relationship trend. 46,47 The PL intensities increase more rapidly at lower incident power densities than higher power densities; in other words, the power-dependent PL intensity becomes saturating. This reflects the fact that the dominating portions of the PL are from the visible emissions due to DAP optical transitions. Since the number of these defects are fixed, the PL saturation at a higher pumping power shall happen. It is also noted that besides the UV_I emission mentioned previously for sample #1, one UV_{II} emission located at \sim 282.71 nm emerges at 14 K, as shown in Fig. 3(a), and other temperatures as shown in Fig. 4(a) later, which may be assigned to the recombination of electrons in the conduction band and holes in the defect complex acceptor level V_{Ga-O} [Fig. S4(b)]. The estimated V_{Ga-O} complex acceptor energy is $\sim\!4.39\,\mathrm{eV}$ below the conduction band, which is close to the reported value of $\sim\!4.42\,\mathrm{eV}$ below the conduction band. With the V_{Ga-O} energy and observed visible emission energies, the three oxygen vacancy deep donor levels are estimated as $\sim\!1.3$, 1.8, and 2 eV below the conduction band edge. These numbers are in reasonable agreement with the reported values of $\beta\!-\!\mathrm{Ga}_2\mathrm{O}_3$.

Figures 4(a)-4(d) show the temperature-dependent PL spectra of samples #1-#4, respectively. The temperature range is between 14 and 300 K, and incident lasing power density is 12.8 mW/cm². Figures 4(e)-4(h) show integrated PL intensity as a function of temperature for the four samples, respectively. For sample #1, PL intensity decreases monotonically vs the temperature in both ranges of 14-40 K and 100-300 K, which is similar to the reported PL spectra trend of β-Ga₂O₃. However, PL intensity increases with temperature in the range of 40-100 K. Similarly, the PL intensity of three spinel MgGa₂O₄ samples first increases with temperature in the range of 14-150 K and then decreases after 150 K until room temperature. At higher temperatures, the integrated PL intensity of all samples decreases as the increase in temperature, which is due to the positive thermal quenching (PTQ) effect. 49,50 Similar phenomena were observed in other materials including GaAs,⁵⁰ ZnO nanorods,⁵¹ and GaSb.⁵² At lower temperatures, the PL intensity increases with the increase in temperature in these samples, especially in spinel MgGa₂O₄ samples, which is due to the negative thermal quenching (NTQ) effect.^{50–52} Based on the multi-level model proposed by Shibata 50 and Wu $\it et~al., ^{51}$ the relationship between PL intensity and temperature can be expressed as $I(T) = I(0) \frac{1 + \sum_{q=1}^{w} D_q \exp(-E_q/k_B T)}{1 + \sum_{j=1}^{m} C_j \exp(-E_j/k_B T)}$, where k_B is the Boltzmann constant,

T is the temperature, E_j (E_q') is the activation energy, and C_j (D_q) is the corresponding weight factor. In this equation, the denominator exponential item is related to the normal PTQ process, namely, as the temperature increases, the PL intensity decreases. This applies to most

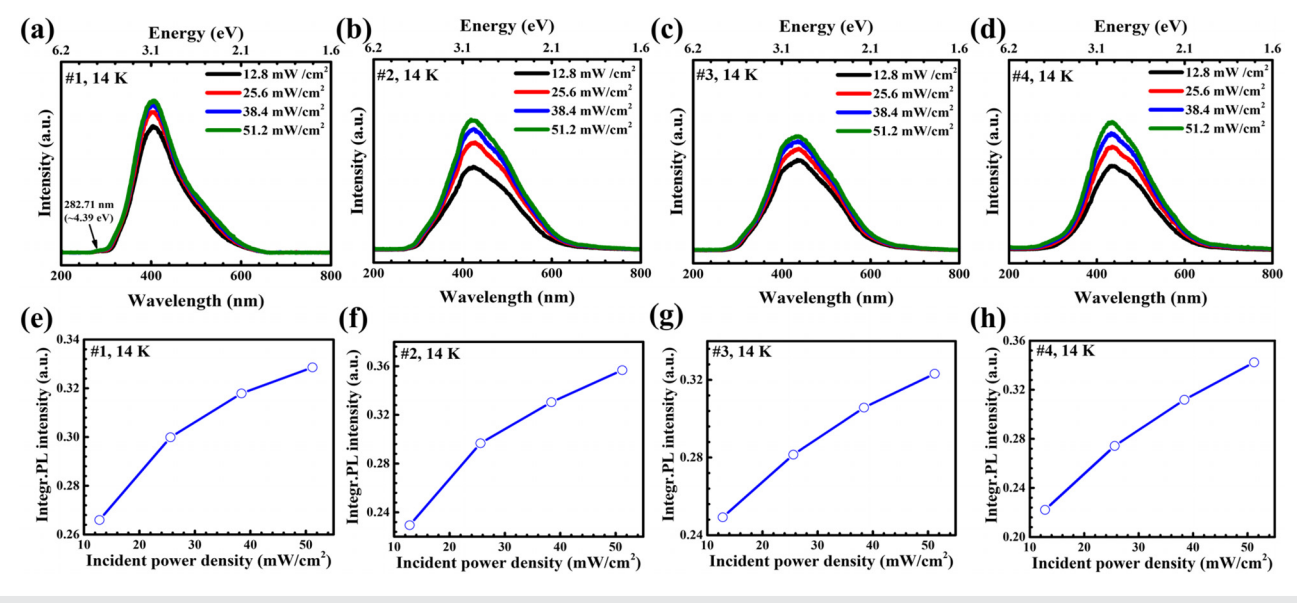


FIG. 3. (a)-(d) Power dependent PL spectra of samples #1-#4, respectively. (e)-(h) Integrated PL intensity vs incident power density for samples #1-#4, respectively.

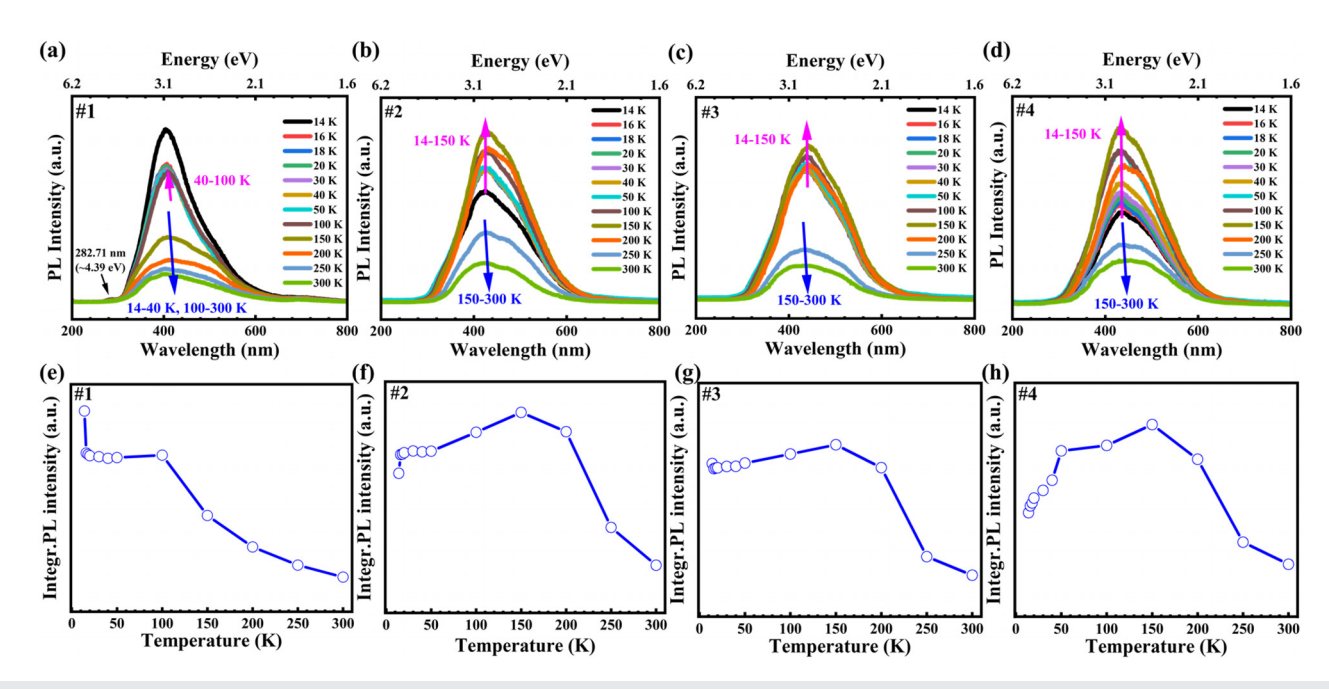


FIG. 4. (a)-(d) Temperature dependent PL spectra of samples #1-#4, respectively. (e) and (f) Integrated PL intensity vs temperature for samples #1-#4, respectively.

direct semiconductors in which there are a few or none defect-related intermediate energy levels that also participate radiative recombination. On the other hand, the numerator exponential item is related to the NTQ effect. The inclusion of this numerator term is related to the existence of intermediate energy levels, which participate radiative recombination processes. The competition of the denominator and numerator terms leads to the above-mentioned observed temperaturedependent PL. Therefore, the NTQ effect here is a direct proof of the PL mechanism in Fig. 2(c), where multiple energy levels in the forbidden gap, which are three oxygen vacancies donor bands, STH level, and Mg on the Ga site MgGa acceptor level, are involved in the PL emissions. To be more specific for both β-Ga₂O₃ and spinel MgGa₂O₄ samples, the electrons trapped in oxygen vacancy donor bands may be re-excited from lower energy levels to higher energy levels or the conduction band to enhance both UV and visible emissions when temperature is low. For higher temperatures, the non-radiative SRH process becomes more dominating; thus, the temperature-dependent PL follows the normal PTQ trend.

In summary, UWBG semiconductors are essential materials for power electronics, deep-UV photonics, and other emerging applications. As one of these promising materials, epitaxial films of spinel MgGa₂O₄ were achieved by MBE. The bandgap was determined to be approximately 5.4–5.5 eV, with high transparency (>90%) in the visible spectral range. The photoluminescence properties of MgGa₂O₄ were extensively studied, encompassing both power and temperature dependence analyses. The PL mechanisms were elucidated, highlighting transitions involving self-trapped holes, oxygen vacancy deep donors, and magnesium atoms on gallium site deep acceptors. On the one hand, the findings underscore the feasibility of using MBE for the epitaxial growth of MgGa₂O₄ films, expanding the repertoire of techniques available for advancing its electronic and optoelectronic device

functionalities. On the other hand, it contributes valuable insights into the optical behavior and native defects studies on $MgGa_2O_4$.

See the supplementary material for the detailed results of MBE growth conditions, SEM cross section and surface morphology of samples #1–#3, XRD and RHEED properties for thickness dependent samples, room temperature PL peak deconvolution of samples #2 and #3, and room temperature PL peak deconvolution and PL mechanism schematic of β -Ga₂O₃ sample #1.

This work was supported by the National Science Foundation (No. ECCS-2105566) and the Air Force Office of Scientific Research under Award No. FA9550-22-1-0505. The authors acknowledge the use of facilities and instrumentation at the UC Irvine Materials Research Institute (IMRI), which is supported in part by the National Science Foundation through the UC Irvine Materials Research Science and Engineering Center (No. DMR-2011967). J.T. and P.W. would like to acknowledge NSF under Award No. NSF CAREER-2046648.

AUTHOR DECLARATIONS Conflict of Interest

The authors have no conflicts to disclose.

Author Contributions

Tianchen Yang: Conceptualization (lead); Data curation (lead); Formal analysis (lead); Investigation (lead); Methodology (lead); Project administration (lead); Resources (lead); Software (lead); Supervision (lead); Validation (lead); Visualization (lead); Writing –

original draft (lead); Writing – review & editing (lead). Chengyun Shou: Conceptualization (supporting); Data curation (supporting); Investigation (supporting); Software (supporting). Jason Tran: Data curation (supporting); Resources (supporting); Software (supporting); Writing – review & editing (supporting). Abdullah Almujtabi: Data curation (supporting); Software (supporting). Quazi Sanjid Mahmud: Software (supporting). Edward Zhu: Software (supporting). Yuan Li: Software (supporting). Peng Wei: Resources (supporting); Writing – review & editing (supporting). Jianlin Liu: Conceptualization (lead); Funding acquisition (lead); Investigation (supporting); Project administration (lead); Supervision (lead); Writing – review & editing (equal).

DATA AVAILABILITY

The data that support the findings of this study are available from the corresponding author upon reasonable request.

REFERENCES

- ¹I. Makkonen, E. Korhonen, V. Prozheeva, and F. Tuomisto, "Identification of vacancy defect complexes in transparent semiconducting oxides ZnO, In₂O₃ and SnO₂," J. Phys. **28**(22), 224002 (2016).
- ²Z. Galazka, D. Klimm, K. Irmscher, R. Uecker, M. Pietsch, R. Bertram, M. Naumann, M. Albrecht, A. Kwasniewski, R. Schewski, and M. Bickermann, "MgGa₂O₄ as a new wide bandgap transparent semiconducting oxide: Growth and properties of bulk single crystals," Phys. Status Solidi A 212(7), 1455–1460 (2015).
- ³E. Ş. Tüzemen, S. Eker, H. Kavak, and R. Esen, "Dependence of film thickness on the structural and optical properties of ZnO thin films," Appl. Surf. Sci. 255(12), 6195–6200 (2009).
- ⁴A. C. Saritha, M. R. Shijeesh, L. S. Vikas, R. R. Prabhu, and M. K. Jayaraj, "Growth and characterization of p-ZnO:Cu thin film and its homojunction application," J. Phys. D **49**(29), 295105 (2016).
- ⁵W. Cheng, Y. He, R. Wei, L. Hu, W. Song, X. Zhu, and Y. Sun, "Transparent p-n heterojunction thin film diodes based on p-CuCrO₂ and n-In₂O₃," Thin Solid Films **781**, 139986 (2023).
- ⁶J. Yang, Z. Yang, T. Meng, Y. Han, X. Wang, and Q. Zhang, "Effects of silicon doping on the performance of tin oxide thin film transistors," Phys. Status Solidi A 213(4), 1010–1015 (2016).
- ⁷Z. Galazka, R. Uecker, D. Klimm, K. Irmscher, M. Pietsch, R. Schewski, M. Albrecht, A. Kwasniewski, S. Ganschow, D. Schulz, C. Guguschev, R. Bertram, M. Bickermann, and R. Fornari, "Growth, characterization, and properties of bulk SnO₂ single crystals," Phys. Status Solidi A 211(1), 66–73 (2014).
- ⁸Z. Galazka, S. Ganschow, K. Irmscher, D. Klimm, M. Albrecht, R. Schewski, M. Pietsch, T. Schulz, A. Dittmar, A. Kwasniewski, R. Grueneberg, S. B. Anooz, A. Popp, U. Juda, I. M. Hanke, T. Schroeder, and M. Bickermann, "Bulk single crystals of β-Ga₂O₃ and Ga-based spinels as ultra-wide bandgap transparent semiconducting oxides," Prog. Cryst. Growth Charact. Mater. **67**(1), 100511 (2021).
- ⁹X. Zhao, W. Cui, Z. Wu, D. Guo, P. Li, Y. An, L. Li, and W. Tang, "Growth and characterization of Sn doped β -Ga₂O₃ thin films and enhanced performance in a solar-blind photodetector," J. Electron. Mater. **46**(4), 2366–2372 (2017).
- 10 T. Yang, C. Shou, L. Xu, J. Tran, Y. He, Y. Li, P. Wei, and J. Liu, "Metal–semi-conductor–metal photodetectors based on β-MgGaO thin films," ACS Appl. Electron. Mater. 5(4), 2122–2130 (2023).
- ¹¹C. Shou, T. Yang, A. Almujtabi, T. Yang, Y. Li, Q. S. Mahmud, M. Xu, J.-G. Zheng, and J. Liu, "Improving crystal quality of β -phase MgGaO thin films by using low-temperature homo-buffer layer," Appl. Phys. Lett. **122**(21), 212101 (2023).
- ¹²T. Yang, C. Shou, A. Almujtabi, J. Tran, Q. Lin, Y. Li, Q. S. Mahmud, P. Wei, and J. Liu, "Investigation of phase transition and ultrawide band gap engineering in MgGaO semiconductor thin films," ACS Appl. Opt. Mater. 1(10), 1670–1678 (2023).

- ¹⁸Q. Hou, K. Liu, X. Chen, J. Yang, Q. Ai, Z. Cheng, Y. Zhu, B. Li, L. Liu, and D. Shen, "Effects of Mg component ratio on photodetection performance of MgGa₂O₄ solar-blind ultraviolet photodetectors," Phys. Status Solidi RRL 16(8), 2200137 (2022).
- ¹⁴Q. Guo, J. Tetsuka, Z. Chen, M. Arita, K. Saito, and T. Tanaka, "Low temperature growth of MgGa₂O₄ films for deep ultraviolet photodetectors," Opt. Mater. 143, 114267 (2023).
- ¹⁵Q. Hou, K. Liu, D. Han, Y. Zhu, X. Chen, B. Li, L. Liu, and D. Shen, "MOCVD growth of MgGa₂O₄ thin films for high-performance solar-blind UV photodetectors," Appl. Phys. Lett. 120(1), 011101 (2022).
- ¹⁶B. Thielert, C. Janowitz, Z. Galazka, and M. Mulazzi, "Theoretical and experimental investigation of the electronic properties of the wide band-gap transparent semiconductor MgGa₂O₄," Phys. Rev. B 97(23), 235309 (2018).
- ¹⁷C. Hirschle, J. Schreuer, and Z. Galazka, "Interplay of cation ordering and thermoelastic properties of spinel structure MgGa₂O₄," J. Appl. Phys. 124(6), 065111 (2018).
- ¹⁸S. Choi, K. Kim, Y.-M. Moon, B.-Y. Park, and H.-K. Jung, "Rapid synthesis of spherical-shaped green-emitting MgGa₂O₄:Mn²⁺ phosphor via spray pyrolysis," Mater. Res. Bull. 45(8), 979–981 (2010).
- 19 A. Luchechko, O. Kravets, L. Kostyk, and O. Tsvetkova, "Luminescence spectroscopy of Eu $^{3+}$ and Mn $^{2+}$ ions in MgGa $_2\mathrm{O}_4$ spinel," Radiat. Meas. 90, 47–50 (2016).
- $^{\bf 20}$ B.-S. Tsai, Y.-H. Chang, and Y.-C. Chen, "Nanostructured red-emitting $MgGa_2O_4:Eu^{3+}$ phosphors," J. Mater. Res. 19(5), 1504–1508 (2004).
- ²¹A. Mondal and J. Manam, "Structural and luminescent properties of Si⁴⁺ co-doped MgGa₂O₄:Cr³⁺ near infra-red long lasting phosphor," ECS J. Solid State Sci. Technol. 6(7), R88 (2017).
- ²²Y. Wang, G. Pan, J. Wang, Y. Li, Z. Wu, S. Xu, and G. Bai, "Simultaneous NIR photoluminescence and mechanoluminescence from Cr³⁺ activated MgGa₂O₄ phosphors with multifunctions for optical sensing," J. Mater. Chem. C 12(10), 3654–3661 (2024).
- ²³A. Mondal, S. Das, and J. Manam, "Hydrothermal synthesis, structural and luminescent properties of a Cr³⁺ doped MgGa₂O₄ near-infrared long lasting nanophospor," RSC Adv. 6(86), 82484–82495 (2016).
- ²⁴G. Zhang, A. Goldstein, and Y. Wu, "Novel transparent MgGa₂O₄ and Ni²⁺-doped MgGa₂O₄ ceramics," J. Adv. Ceram. 11(3), 470–481 (2022).
- ²⁵D. V. Mlotswa, L. L. Noto, S. J. Mofokeng, K. O. Obodo, V. R. Orante-Barrón, and B. M. Mothudi, "Luminescence dynamics of MgGa₂O₄ prepared by solution combustion synthesis," Opt. Mater. 109, 110134 (2020).
- ²⁶Z. Liu, P. Hu, X. Jing, and L. Wang, "Luminescence of native defects in MgGa₂O₄," J. Electrochem. Soc. 156(1), H43 (2009).
- **27**R. Jangir, S. Porwal, P. Tiwari, P. Mondal, S. K. Rai, A. K. Srivastava, I. Bhaumik, and T. Ganguli, "Correlation between surface modification and photoluminescence properties of β -Ga₂O₃ nanostructures," AIP Adv. **6**(3), 035120 (2016).
- ²⁸K. Zhang, Z. Xu, S. Zhang, H. Wang, H. Cheng, J. Hao, J. Wu, and F. Fang, "Raman and photoluminescence properties of un-/ion-doped β -Ga₂O₃ single-crystals prepared by edge-defined film-fed growth method," Physica B **600**, 412624 (2021).
- ²⁹K. Zhang, Z. Xu, J. Zhao, H. Wang, J. Hao, S. Zhang, H. Cheng, and B. Dong, "Temperature-dependent Raman and photoluminescence of β -Ga₂O₃ doped with shallow donors and deep acceptors impurities," J. Alloys Compd. **881**, 160665 (2021).
- 30 B. A. Scott, K. H. Nichols, R. M. Potemski, and J. M. Woodall, "Magnesium gallate spinel: A substrate for the direct liquid-phase epitaxial growth of (Ga, Al) As," Appl. Phys. Lett. 21(4), 121–122 (1972).
- ³¹X. Yu, X. Yang, J. Huan, J. Tong, Y. Qiao, J. Xing, Z. Zhang, and J. Zhao, "Intense NIR mechanoluminescence from Al³⁺-regulated MgGa₂O₄: Cr³⁺," Chem. Eng. J. 491, 152155 (2024).
- ³²G. Katz and R. Roy, "Solid state crystal growth of the spinel MgGa₂O₄," J. Cryst. Growth 6(3), 221–227 (1970).
- ³³A. Luchechko and O. Kravets, "Synthesis and luminescent properties of magnesium gallate spinel doped with Mn²⁺ and Eu³⁺ ions," Phys. Status Solidi C 14(1-2), 1600146 (2017).
- 34 T. Suzuki, M. Hughes, and Y. Ohishi, "Optical properties of Ni-doped MgGa₂O₄ single crystals grown by floating zone method," J. Lumin. 130(1), 121–126 (2010).

- ³⁵M. A. Hamid, B. Samuels, S. Karmakar, M. A. Halim, I. H. Emu, P. K. Sarkar, M. F. N. Taufique, A. Haque, and R. Droopad, "Epitaxial growth and characterization of magnesium gallate (MgGa₂O₄) thin films by pulsed laser deposition," J. Alloys Compd. 972, 172807 (2024).
- ³⁶G. Pilania, V. Kocevski, J. A. Valdez, C. R. Kreller, and B. P. Uberuaga, "Prediction of structure and cation ordering in an ordered normal-inverse double spinel," Commun. Mater. 1(1), 84 (2020).
- ³⁷Y. K. Frodason, K. M. Johansen, L. Vines, and J. B. Varley, "Self-trapped hole and impurity-related broad luminescence in β-Ga₂O₃," J. Appl. Phys. 127(7), 075701 (2020).
- ³⁸S. Marcinkevičius and J. S. Speck, "Ultrafast dynamics of hole self-localization in β -Ga₂O₃," Appl. Phys. Lett. **116**(13), 132101 (2020).
- ³⁹T. Gake, Y. Kumagai, and F. Oba, "First-principles study of self-trapped holes and acceptor impurities in Ga₂O₃ polymorphs," Phys. Rev. Mater. **3**(4), 044603 (2019).
- 40]. L. Lyons, A. Janotti, and C. G. Van de Walle, "Effects of hole localization on limiting *p*-type conductivity in oxide and nitride semiconductors," J. Appl. Phys. 115(1), 012014 (2014).
- ⁴¹Y. Wang, P. T. Dickens, J. B. Varley, X. Ni, E. Lotubai, S. Sprawls, F. Liu, V. Lordi, S. Krishnamoorthy, S. Blair, K. G. Lynn, M. Scarpulla, and B. Sensale-Rodriguez, "Incident wavelength and polarization dependence of spectral shifts in β-Ga₂O₃UV photoluminescence," Sci. Rep. 8(1), 18075 (2018).
- ⁴²J. B. Varley, A. Janotti, C. Franchini, and C. G. Van de Walle, "Role of self-trapping in luminescence and *p*-type conductivity of wide-band-gap oxides," Phys. Rev. B 85(8), 081109 (2012).
- 43 X. Zhu, Y.-W. Zhang, S.-N. Zhang, X.-Q. Huo, X.-H. Zhang, and Z.-Q. Li, "Defect energy levels in monoclinic β-Ga₂O₃," J. Lumin. **246**, 118801 (2022).

- ⁴⁴F. X. Xiu, Z. Yang, L. J. Mandalapu, D. T. Zhao, J. L. Liu, and W. P. Beyermann, "High-mobility Sb-doped *p*-type ZnO by molecular-beam epitaxy," Appl. Phys. Lett. 87(15), 152101 (2005).
- ⁴⁵B. Jiang, F. Chi, X. Wei, Y. Chen, and M. Yin, "A self-activated MgGa₂O₄ for persistent luminescence phosphor," J. Appl. Phys. 124(6), 063101 (2018).
 ⁴⁶A. Sabbar, S. Madhusoodhanan, S. Al-Kabi, B. Dong, J. Wang, S. Atcitty, R.
- ⁴⁶A. Sabbar, S. Madhusoodhanan, S. Al-Kabi, B. Dong, J. Wang, S. Atcitty, R. Kaplar, D. Ding, A. Mantooth, S.-Q. Yu, and Z. Chen, "High temperature and power dependent photoluminescence analysis on commercial lighting and display LED materials for future power electronic modules," Sci. Rep. 9(1), 16758 (2019).
- ⁴⁷j. B. Cui and M. A. Thomas, "Power dependent photoluminescence of ZnO," J. Appl. Phys. 106(3), 033518 (2009).
- ⁴⁸D. Hu, S. Zhuang, Z. Ma, X. Dong, G. Du, B. Zhang, Y. Zhang, and J. Yin, "Study on the optical properties of β -Ga₂O₃ films grown by MOCVD," J. Mater. Sci. **28**(15), 10997–11001 (2017).
- ⁴⁹V. A. Fonoberov, K. A. Alim, A. A. Balandin, F. Xiu, and J. Liu, "Photoluminescence investigation of the carrier recombination processes in ZnO quantum dots and nanocrystals," Phys. Rev. B 73(16), 165317 (2006).
- ⁵⁰H. Shibata, "Negative thermal quenching curves in photoluminescence of solids," Jpn. J. Appl. Phys., Part 1 37(2R), 550 (1998).
- ⁵¹Y. Wu, J. Li, H. Ding, Z. Gao, Y. Wu, N. Pan, and X. Wang, "Negative thermal quenching of photoluminescence in annealed ZnO-Al₂O₃ core-shell nanorods," Phys. Chem. Chem. Phys. 17(7), 5360-5365 (2015).
- ⁵²J. H. Park, T. K. Lee, Y. K. Noh, M. D. Kim, and E. Oh, "Temperature and excitation power dependence of photoluminescence from high quality GaSb grown on AlSb and GaSb buffer layers," J. Appl. Phys. 105(4), 043516 (2009).